Journal of Materials Chemistry C

ROYAL SOCIETY OF CHEMISTRY

PAPER

View Article Online
View Journal | View Issue

Cite this: J. Mater. Chem. C, 2020, 8, 15253

Engineering functionalized low LUMO [1]benzothieno[3,2-*b*][1]benzothiophenes (BTBTs): unusual molecular and charge transport properties†

Resul Ozdemir, ‡[a] Kyunghan Ahn, ‡[b] İbrahim Deneme,[a] Yunus Zorlu,[c] Dojun Kim,[b] Myung-Gil Kim[b] and Hakan Usta *[a]

Diacene-fused thienothiophenes (DAcTTs) have provided an excellent π-framework for the development of high mobility p-type molecular semiconductors in the past decade. However, n-type DAcTTs are rare and their electron transport characteristics remain largely unexplored. Herein, a series of functionalized low LUMO (lowest unoccupied molecular orbital) [1]benzothieno[3,2-*b*][1]benzothiophene (BTBT)-based small molecules, **D(C$_7$CO)-BTBT**, **C$_7$CO-BTBT-CC(CN)$_2$C$_7$**, and **D(C$_7$CC(CN)$_2$)-BTBT**, have been developed. Detailed structural, physicochemical, optoelectronic, and single-crystal characterization were performed. The new molecules exhibit large optical band gaps (~2.8–3.1 eV) and highly stabilized ($-\Delta E_{LUMO}$ = 1.2–1.4 eV)/π-delocalized LUMOs as compared to p-type DAcTTs. Symmetric functionalization is found to be important to enable strong intermolecular interactions in the solid-state. All molecules exhibit alternately stacked layers of "F–BTBT–F" and "S" (F: functional group/S: substituent) with strong herringbone-like interactions (2.8–3.6 Å distances) between π-cores. While carbonyls, regardless of the substituent, adopt nearly coplanar π-backbones with BTBT, dicyanovinylenes are found to be twisted (47.5°). The conformational difference at the molecular level has unusual effects on the π-electron deficiencies, frontier molecular orbital energetics, thermal/photophysical properties, and π-electronic structures. Dicyanovinylenes at the 2,7 positions, despite twisted conformations, are shown for the first time to yield good electron transport in DAcTTs. The **D(C$_7$CC(CN)$_2$)-BTBT** thin film exhibits large 2D plate-like crystalline grains (~1–2 μm sizes) of terraced islands and becomes a rare example of an n-type DAcTT in organic field-effect transistors (OFETs). Although a stabilized/π-delocalized LUMO, largely governed by functional groups and intramolecular twists, is essential for electron transport, our findings suggest that it should be combined with proper substituents to yield a favorable three-dimensional BTBT/functional group π-electronic structure and a low intramolecular reorganization energy. Combined with our first n-type DAcTT semiconductor **D(Ph$_F$CO)-BTBT**, a molecular library with systematically varied chemical structures has been studied herein for the first time for low LUMO DAcTTs. The molecular engineering perspectives presented in this study may give unique insights into the design of novel electron transporting thienoacenes for unconventional optoelectronics.

Received 21st June 2020,
Accepted 31st July 2020

DOI: 10.1039/d0tc02945a

rsc.li/materials-c

[a] Department of Materials Science and Nanotechnology Engineering, Abdullah Gül University, Kayseri 38080, Turkey. E-mail: hakan.usta@agu.edu.tr
[b] School of Advanced Materials Science & Engineering, Sungkyunkwan University, Suwon 16419, Republic of Korea
[c] Department of Chemistry, Gebze Technical University, Gebze, Kocaeli 41400, Turkey

† Electronic supplementary information (ESI) available: Theoretical (DFT/B3LYP/6-31G**) HOMO/LUMO energy levels and topographical orbital representations for different functionalization positions of **D(C$_7$CO)-BTBT** and **D(C$_7$CC(CN)$_2$)-BTBT** (Fig. S1 and S2); chemical characterization (^{1}H/^{13}C NMR and MALDI TOF-MS spectra) (Fig. S3–S11); FT-IR spectra (Fig. S12); computationally optimized molecular structures for **D(C$_7$CO)-BTBT**, **D(C$_7$CC(CN)$_2$)-BTBT**, and **D(HCC(CN)$_2$)-BTBT** (Fig. S13 and S14); optical absorption spectrum and cyclic voltammogram of **C$_8$-BTBT** in dichloromethane solutions (Fig. S15); optical absorption spectra in solvents with varied polarities (Fig. S16); theoretical frontier molecular orbital energies/topographical representations for varied conformations of **D(C$_7$CC(CN)$_2$)-BTBT** (Fig. S17); solvent polarity-dependent photoluminescence spectra of **D(C$_7$CC(CN)$_2$)-BTBT** (Fig. S18); simulated XRD powder patterns for **D(C$_7$CO)-BTBT** and **D(C$_7$CC(CN)$_2$)-BTBT** (Fig. S19); grazing incidence X-ray diffraction (GIXD) of the **D(C$_7$CO)-BTBT** thin film deposited at room temperature (Fig. S20). CCDC 1946322 and 1946323. For ESI and crystallographic data in CIF or other electronic format see DOI: 10.1039/d0tc02945a

‡ These authors contributed equally to this work.

Introduction

Organic π-conjugated small molecules with fused rings offer great promise as semiconductors in the fields of fundamental charge transport studies and optoelectronic device applications.[1–12] The earlier approaches to the development of molecular semiconductors have focused on oligomeric π-structures such as oligo-thiophenes/phenylenes as a result of their structural versatility, convenient synthesis, and appreciable charge-transport characteristics.[13–18] However, the realization of fused π-conjugated derivatives has greatly influenced molecular semiconductor developments as a result of their highly advantageous optoelectronic/physicochemical characteristics and much higher charge carrier mobilities compared to oligomers.[3,19,20] The attractive properties of fused π-systems include a coplanar π-backbone with highly delocalized frontier molecular orbitals enabling effective charge injection/extraction and delocalization, low reorganization energies for charge hopping, and very effective intermolecular interactions (large transfer integrals) in the solid-state.[21–24] While the majority of research efforts on fused π-systems have focused on low band-gap acenes and polycyclic aromatic compounds such as pentacene,[25] TIPS-pentacene,[26] and perylenediimide,[27] diacene-fused thienothiophenes (DAcTTs) (*e.g.*, [1]benzothieno[3,2-*b*][1]benzothiophene (BTBT)) have emerged in the past decade as new generation hole transporting (p-type) semiconductors with unprecedented charge carrier mobilities.[28–30] In this type of thienoacenes, the presence of a phene-like electronic structure with large sulfur atoms on the central thieno[3,2-*b*]thiophene enables a unique semiconductor π-structure with a large band gap, stabilized highest occupied molecular orbital (HOMO) energy level, and impressive hole transport ability.[31] Particularly, their vapor-deposited and solution-processed thin films favor two dimensional (2D) in-plane herringbone packing motifs to yield very high hole mobilities in organic field-effect transistors (OFETs).[32,33] Despite these premises, to the best of our knowledge, DAcTTs had never been studied in the design of low (<-3 eV) LUMO (lowest unoccupied molecular orbital) electron transporting (n-type) semiconducting molecules prior to our very recent report.[34] This had raised two critical fundamental questions as to whether functionalization with electron withdrawing functional groups in DAcTTs, which are typically wide band-gap π-cores, could ever enable efficient electron transport and what structure–molecular properties–semiconductivity relationships would be effective. The first question is particularly interesting because almost all p-type π-frameworks including acenes[35] have been tailored to yield n-type semiconductors *via* proper functionalization.[36–38] To realize efficient electron transport from DAcTT derivatives that is as high as their hole mobilities would greatly contribute to the development of complementary organic circuits and wide-ranging optoelectronic applications wherever electron transport is desired.[39–45] It could also open up new opportunities in optoelectronics when combined with DAcTTs' other interesting properties such as relatively easy synthesis (multigram scale), wide optical band gaps (optical transparency), and deep HOMO energies.[23]

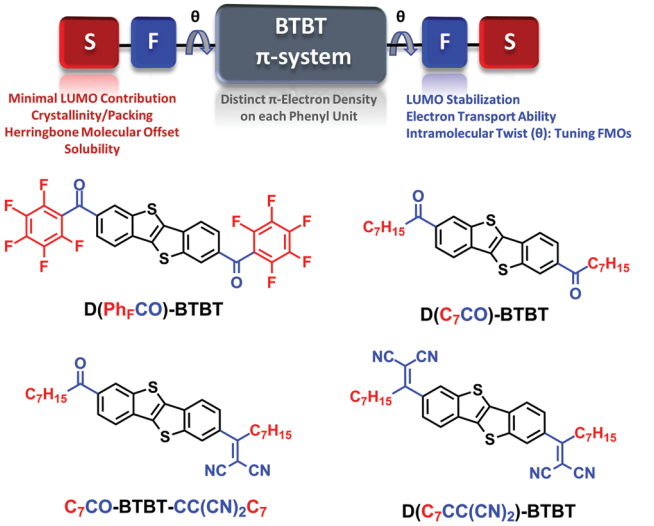

Fig. 1 The S–F–BTBT–F–S (F/S: functional group/substituent) design architecture for functionalized low LUMO BTBT molecules indicating the contributions of each substructure and the chemical structures of **D(C$_7$CO)-BTBT**, **C$_7$CO-BTBT-CC(CN)$_2$C$_7$**, and **D(C$_7$CC(CN)$_2$)-BTBT** developed in this study and **D(Ph$_F$CO)-BTBT**[34] developed in our previous study.

To this end, we have recently demonstrated the first example of an n-type DAcTT semiconductor in the literature, **D(Ph$_F$CO)-BTBT**[34] (Fig. 1), which showed a highly stabilized (E_{LUMO} = −3.64 eV) LUMO as compared to p-type DAcTTs. The OFET devices with highly crystalline **D(Ph$_F$CO)-BTBT** films demonstrated high electron mobilities of $\sim$0.6 cm^2 V^{-1} s^{-1} and I_{on}/I_{off} ratios over 10^7–10^8. Prompted by these initial promising results, we are now interested in engineering new functionalized low LUMO BTBTs in an "S–F–BTBT–F–S (F/S: functional group/substituent)" molecular architecture (Fig. 1) and creating a molecular library to explore structure–molecular properties–semiconductivity relationships in this new class of molecular semiconductors. We are particularly keen to understand the electronic/structural factors governing electron transport in DAcTTs, and how these parameters could be tuned *via* functional groups and substituents. In our present study, BTBT is the preferred π-framework because it is the smallest member of the DAcTT family with good charge transport properties, and functionalization on the BTBT π-core is expected to have an immediate effect on the electronic structure. Also, the BTBT π-core is open to Friedel–Crafts acylations and further functionalization with ease, and its π-structural dimension is very likely to enable solubility *via* proper substitutions. To this end, as shown in Fig. 1, BTBT is systematically functionalized with electron withdrawing carbonyl and dicyanovinylene functional groups (in blue) and substituted with heptyl chains (–C$_7$H$_{15}$) (in red). This design is envisioned to yield a combination of a low LUMO and good solubility for convenient synthesis/purification, and systematic functionalization could reveal the electronic effects of carbonyl *vs.* dicyanovinylene on BTBT's π-electronic structure and electron transport characteristics. The quantum mechanical modeling (DFT, B3LYP/6-31G**) used in the design of these molecules prior to the synthesis points out

that for all compounds, among the four possible symmetric BTBT functionalization positions (1,6/2,7/3,8/4,9), the 2,7-positions give the lowest LUMO energies with the most delocalized wave functions (Fig. S1 and S2, ESI†). The difference becomes especially pronounced in the case of dicyanovinylene functionalization in that all positions other than 2,7 tend to localize the LUMO wave functions on the dicyanovinylene units.

We present herein the design, synthesis, and full characterization of a series of functionalized low LUMO [1]benzothieno[3,2-*b*][1]benzothiophene (BTBT)-based small molecules, **D(C_7CO)-BTBT**, **C_7CO-BTBT-CC(CN)$_2$$C_7$**, and **D($C_7$CC(CN)$_2$)-BTBT** (Fig. 1). Detailed structural, physicochemical, and optoelectronic characterization were performed; the single-crystal structures for **D(C_7CO)-BTBT** and **D(C_7CC(CN)$_2$)-BTBT** were accessed. Note that while **C_7CO-BTBT-CC(CN)$_2$$C_7$** and **D($C_7$CC(CN)$_2$)-BTBT** are novel compounds, **D(C_7CO)-BTBT**[46] has previously been described as an intermediate compound, yet with no OFET characteristics or molecular/single-crystal properties, during the synthesis of p-channel BTBTs. As a result of functionalization with electron withdrawing carbonyl/dicyanovinylene units, the LUMOs are remarkably stabilized ($-\Delta E_{LUMO}$ = 1.2–1.4 eV), while the optical band gaps remain large (2.8–3.1 eV). Thermal and thin film characterization reveal that symmetric functionalization is crucial to enable strong intermolecular interactions in the solid-state. The carbonyl functionalities, regardless of the substituents (*i.e.*, heptyl and pentafluorophenyl), adopt coplanar π-conformations with BTBT. However, dicyanovinylenes are found to be twisted (47.5°), which has unusual effects on the π-electron deficiencies, thermal properties, frontier molecular orbital energetics, photophysical properties, and π-electronic structures. While functional groups and intramolecular twists govern LUMO stabilization/π-delocalization, substituents appear to be the key component to form a favorable three-dimensional π-electronic structure and a low intramolecular reorganization energy for electron transport. In our study, despite their twisted conformations, 2,7-dicyanovinylenes are shown for the first time to yield good electron transport in DAcTTs. **D(C_7CC(CN)$_2$)-BTBT** thin films exhibit large 2D plate-like crystalline grains (~1–2 μm sizes) of terraced islands and it becomes a rare example of an n-type DAcTT with an appreciable μ_e of 0.004 cm^2 V^{-1} s^{-1} (I_{on}/I_{off} = 10^6–10^7) in OFETs. On the basis of these unique findings, structure–molecular properties–semiconductivity relationships are established for the first time in low LUMO DAcTTs.

Experimental

Materials and methods

Conventional Schlenk techniques were used for the reactions performed under an N_2 atmosphere. All of the chemicals were purchased from commercial sources and used without further purification unless otherwise noted. Column chromatography was carried out using 230–400 mesh particle size (60 Å pore size) silica gel as the stationary phase. ^{1}H/^{13}C NMR spectra were recorded on a Bruker 400 spectrometer (^{1}H, 400 MHz; ^{13}C, 100 MHz). Elemental analyses were done on a LecoTruspec Micro model instrument. High-resolution mass spectra were measured on a Bruker Microflex LT MALDI-TOF-MS instrument. Thermogravimetric analysis (TGA) and differential scanning calorimetry (DSC) measurements were performed on Mettler Toledo-TGA/STDA 851 and Mettler Toledo-DSC 821 model instruments, respectively, at a heating rate of 10 °C min^{-1} under a nitrogen atmosphere. UV-vis absorption spectra were recorded *via* a Shimadzu UV-1800 spectrophotometer. Photoluminescence (PL) characterization was carried out with an Agilent-Cary Eclipse fluorescence spectrophotometer. Time-correlated single photon counting measurements were performed using a Pico Quant FluoTime 200 equipped with a 375 nm pulsed (200 ps pulse width) laser diode. The PL quantum yields in solution were measured using the comparative method with a standard fluorescent Coumarin 153 dye solution (Φ_{PL} = 53% in ethanol).[47,48] Electrochemical characterization was carried out *via* cyclic voltammetry measurements on a C3 Cell Stand electrochemical station equipped with BAS-Epsilon software (Bioanalytical Systems, Inc. Lafayette, IN). The working and counter electrodes were Pt, and the reference electrode was Ag/AgCl (3 M NaCl). All the potentials were calibrated with respect to the standard ferrocene/ferrocenium redox couple (Fc/Fc$^+$: $E_{1/2}$ = +0.40 V measured in the same electrochemical set-up). The optimization of the molecular geometries and the analysis of the frontier molecular orbitals were carried out in Gaussian 09 using density functional theory (DFT) at the B3LYP/6-31G** level.[49] The intramolecular reorganization energies for hole (λ_h) and electron (λ_e) transfer for **D(Ph_FCO)-BTBT** and **D(C_7CO)-BTBT** were calculated in accordance with a standard procedure reported in the literature.[50]

Synthesis and structural characterization

The synthesis of [1]benzothieno[3,2-*b*][1]benzothiophene (BTBT) was carried out in accordance with the reported procedure.[46,51]

Synthesis of 1,1′-(benzo[*b*]benzo[4,5]thieno[2,3-*d*]thiophene-2,7-diyl)bis(octan-1-one) (D(C_7CO)-BTBT). $AlCl_3$ (3.03 g, 22.76 mmol) was added into a solution of [1]benzothieno[3,2-*b*][1]benzothiophene (1.0 g, 4.16 mmol) in anhydrous dichloromethane (100 mL) at −10 °C under nitrogen. The resulting solution was stirred at −10 °C for 30 min. Then, the reaction mixture was cooled down to −78 °C. Octanoyl chloride (3.38 g, 20.8 mmol) was subsequently added dropwise, and the mixture was stirred for 1 h at the same temperature. The reaction mixture was allowed to warm to room temperature and stirred for 2 days. After completing the reaction, the mixture was quenched with water to give a white precipitate. The precipitate was collected by filtration, and then washed with water and methanol, respectively. The product was obtained as a pale yellow solid (1.2 g, 58% yield). The compound was directly used in the next step without any further purification. For OFET device fabrication, 100 mg of this crude solid was purified *via* column chromatography on silica gel using chloroform as a mobile phase to afford the pure semiconductor solid (80 mg). Melting point: 265–266 °C; ^{1}H NMR (400 MHz, $CDCl_3$), δ (ppm): 8.59 (s, 2H), 8.09 (d, 2H, J = 8.0 Hz), 7.98 (d, 2H, J = 8.0 Hz), 3.08 (t, 4H, J = 12.0 Hz), 1.78–1.85 (m, 4H), 1.33–1.44 (m, 16H), 0.89–0.93 (t, 6H, J = 16.0 Hz); ^{13}C NMR (100 MHz, $CDCl_3$), δ (ppm):

199.5, 142.8, 136.2, 135.8, 134.3, 124.9, 124.6, 121.9, 38.9, 31.7, 29.4, 29.2, 24.5, 22.6, 14.1; MS (MALDI-TOF) *m*/*z* calcd for $C_{30}H_{36}O_2S_2$: 492.22 [M^+]; found: 492.44 [M^+]; elemental analysis calcd (%) for $C_{30}H_{36}O_2S_2$: C, 73.13; H, 7.36; found: C, 73.46; H, 7.67.

Synthesis of 2-(1-(7-octanoylbenzo[*b*]benzo[4,5]thieno[2,3-*d*]-thiophen-2-yl)octylidene) malononitrile (C_7CO-BTBT-CC(CN)$_2C_7$). Piperidine (0.73 g, 8.51 mmol) was added into a solution of 1,1′-(benzo[*b*]benzo[4,5]thieno[2,3-*d*]thiophene-2,7-diyl)bis(octan-1-one) (**D(C_7CO)-BTBT**) (0.50 g, 1.01 mmol), and malononitrile (0.97 g, 14.61 mmol) in 50 mL of anhydrous DMSO under nitrogen. The resulting mixture was stirred at 110 °C for 2 hours. After completing the reaction, it was allowed to cool down to room temperature. The reaction mixture was quenched with water. After extraction with $CHCl_3$, the organic layer was dried with Na_2SO_4, filtered and concentrated to obtain the crude product. The crude was then purified through column chromatography on silica gel using chloroform as the mobile phase to afford the final product as a yellow solid (110 mg, 20% yield). Melting point: 102–103 °C; ^{1}H NMR (400 MHz, $CDCl_3$), δ (ppm): 8.59 (s, 1H), 8.10–8.12 (d, 2H, J = 8.0 Hz), 8.05–8.07 (d, 1H, J = 8.0 Hz), 7.99–8.01 (d, 1H, J = 8.0 Hz), 7.59–7.62 (d, 1H, J = 12.0 Hz), 3.06–3.11 (m, 4H), 1.78–1.85 (m, 2H), 1.24–1.49 (m, 18H), 0.84–0.92 (m, 6H); ^{13}C NMR (100 MHz, $CDCl_3$), δ (ppm): 199.5, 179.5, 143.2, 142.9, 135.6, 135.3, 134.5, 131.9, 124.6, 123.5, 122.6, 121.9, 112.9, 112.6, 84.8, 38.9, 37.8, 31.7, 31.5, 29.4, 29.2, 22.6, 22.5, 14.1, 14.0; MS (MALDI-TOF) *m*/*z* calcd for $C_{33}H_{36}N_2OS_2$: 540.23 [M^+]; found: 540.34 [M^+]; elemental analysis calcd (%) for $C_{33}H_{36}N_2OS_2$: C, 73.29; H, 6.71; N, 5.18; found: C, 73.47; H, 6.88; N, 5.01.

Synthesis of 2,2′-(benzo[*b*]benzo[4,5]thieno[2,3-*d*]thiophene-2,7-diylbis(octan-1-yl-1-ylidene))dimalononitrile (D(C_7CC(CN)$_2$)-BTBT). A mixture of 1,1′-(benzo[*b*]benzo[4,5]thieno[2,3-d]thiophene-2,7-diyl)bis(octan-1-one) (**D(C_7CO)-BTBT**) (0.25 g, 0.51 mmol) and malononitrile (0.47 g, 7.14 mmol) was dissolved in anhydrous chlorobenzene (50 mL) under nitrogen, and stirred at 35 °C for 15 min. Afterwards, pyridine (0.77 g, 9.69 mmol) and $TiCl_4$ (0.97 g, 5.1 mmol) were added to the reaction mixture. The resulting mixture was heated and stirred at 110 °C for 90 min. After completing the reaction, it was allowed to cool down to room temperature. The reaction mixture was quenched with water. After extraction with $CHCl_3$, the organic layer was dried with Na_2SO_4, filtered and concentrated to obtain the crude product. The crude was then purified through column chromatography on silica gel using CH_2Cl_2 as a mobile phase to afford the final product as a pale yellow solid (138 mg, 46% yield). Melting point: 211–212 °C; ^{1}H NMR (400 MHz, $CDCl_3$), δ (ppm): 8.10 (s, 2H), 8.05–8.07 (d, 2H, J = 8.0 Hz), 7.60–7.62 (d, 2H, J = 8.0 Hz), 3.06–3.10 (t, 4H, J = 16.0 Hz), 1.34–1.41 (m, 4H), 1.24–1.32 (m, 16H), 0.84–0.87 (t, 6H, J = 12.0 Hz); ^{13}C NMR (100 MHz, $CDCl_3$), δ (ppm): 179.5, 143.3, 135.9, 135.1, 132.2, 124.4, 123.5, 122.6, 112.9, 112.5, 85.0, 37.9, 31.5, 29.1, 28.7, 28.6, 22.5, 14.0; MS (MALDI-TOF) *m*/*z* calcd for $C_{36}H_{36}N_4S_2$: 588.24 [M^+]; found: 588.52 [M^+]; elemental analysis calcd (%) for $C_{36}H_{36}N_4S_2$: C, 73.43; H, 6.16; N, 9.51; found: C, 73.74; H, 6.44; N, 9.42.

Field-effect transistor fabrication and characterization

Heavily n-doped (100) silicon (n^{++}-Si) with 200 nm thermally grown SiO_2 was used as the gate/dielectric substrate for OFET fabrication. The substrates were sonicated in acetone and isopropyl alcohol for 10 min with subsequent drying under an N_2 flow. Then, the substrates were treated with 100 W oxygen plasma for 3 min (Cute, Femto Science, South Korea). To form the hydrophobic interfacial layer, n^{++}-Si/SiO_2 (200 nm) substrates were treated with hexamethyldisilazane (HMDS). To deposit 30 nm thick organic semiconductor films, the **D(C_7CO)-BTBT** and **D(C_7CC(CN)$_2$)-BTBT** solids were thermally evaporated onto temperature-controlled (25 °C and 70 °C) n^{++}-Si/SiO_2 (200 nm)/HMDS substrates under a high vacuum ($\sim 10^{-6}$ Torr) using a growth rate of 0.1–0.2 Å s^{-1}. The surface morphology and microstructure of the evaporated semiconductor thin-films were characterized by atomic force microscopy (AFM, NX10, Park Systems, South Korea) and grazing incidence X-ray diffraction (GIXRD, X'pert Pro, Malvern Panalytical Ltd). The source–drain electrodes (LiF (1 nm)/Au (50 nm) for n-channel testing and Au (50 nm) for p-channel testing) were defined *via* thermal evaporation through a shadow mask to yield semiconducting channels of 1000 μm width and 50 μm length. The semiconductor channels were electrically isolated from each other using a mechanical scratch. The electrical characterization of the OFETs was performed in a vacuum probe station (M5VC, MSTech, South Korea) using a Keithley 4200-SCS semiconductor analyzer system (Tektronix Inc, USA). The saturation charge carrier mobility (μ_{sat}) was estimated based on a conventional metal–oxide–semiconductor field-effect transistor model using the formula

$$\mu_{sat} = (2I_{DS}L)/[WC_i(V_G - V_{th})^2]$$

where I_{DS} is the source–drain current, L is the channel length, W is the channel width, C_i is the areal capacitance of the gate dielectric, V_G is the gate voltage, and V_{th} is the threshold voltage.

Results and discussion

Synthesis, characterization, and thermal properties

The synthesis of the new molecules is shown in Scheme 1. As the first step, **D(C_7CO)-BTBT** was synthesized *via* double Friedel–Crafts acylation with a yield of 58%. Note that this reaction has previously been carried out as an intermediate step in the synthesis of p-type BTBT compounds (*e.g.*, **C_8-BTBT**), and it selectively functionalizes the BTBT π-core at the 2,7-positions.[46,51] Then, Knoevenagel condensations were carried out on **D(C_7CO)-BTBT** to convert carbonyls to dicyanovinylene groups. For single carbonyl conversion, malononitrile reacts with **D(C_7CO)-BTBT** in the presence of piperidine base to yield **C_7CO-BTBT-CC(CN)$_2C_7$** in 20% yield. In the synthesis of **D(C_7CC(CN)$_2$)-BTBT**, $TiCl_4$ Lewis acid was needed along with pyridine and malononitrile to achieve double carbonyl conversion (46% yield). All small molecules exhibit good solubilities in common organic solvents (*e.g.*, >15–20 mg mL^{-1} in chloroform)

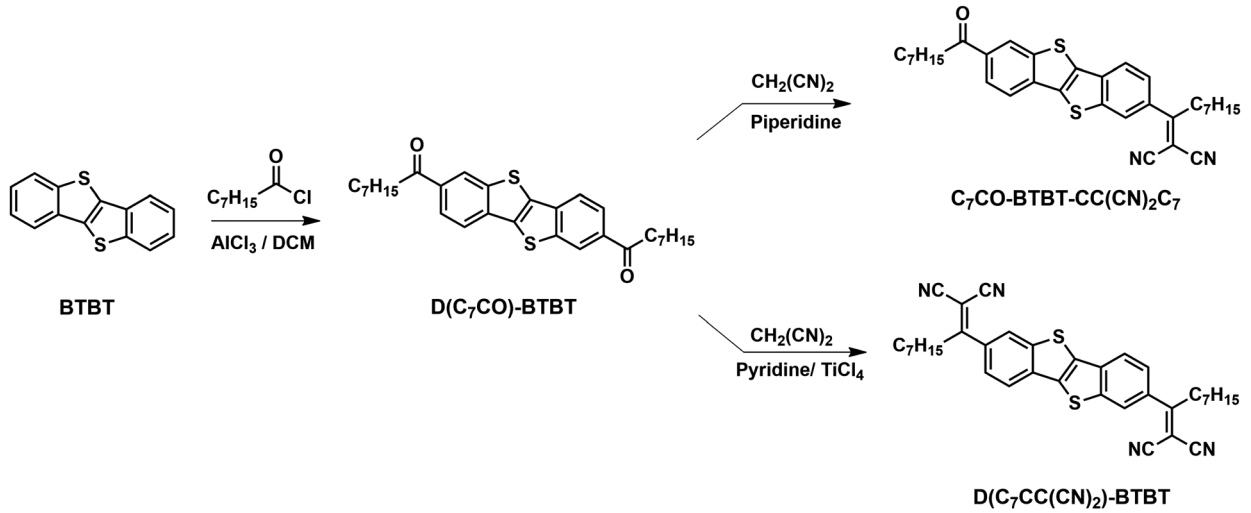

Scheme 1 Synthesis of highly soluble functionalized low LUMO BTBT molecules **D(C_7CO)-BTBT**, **C_7CO-BTBT-CC(CN)$_2C_7$**, and **D(C_7CC(CN)$_2$)-BTBT**.

allowing for convenient synthesis and chromatographic purification. As compared with previously developed **D(Ph_FCO)-BTBT**, which had very low solubility, such good solubilities of the current molecules certainly reflect the solubilizing effect of the flexible alkyl ($-C_7H_{15}$) substituents. Similar to p-channel BTBT derivatives, medium-sized ($-C_nH_{2n+1}$, n = 5–8) linear alkyl chains are sufficient to provide good solubility in functionalized low LUMO BTBT derivatives. It is also noticed that the dicyanovinylene functionalization of the carbonyl unit improves the solubility, which could be ascribed to the increased local dipoles and the twisted molecular conformation as evidenced from the DFT calculations and the single-crystal structures (*vide infra*).

The molecular structures and chemical purities were characterized by using ^{1}H and ^{13}C NMR spectroscopies (Fig. S3, S4, S6, S7, S9, and S10, ESI†), MALDI-TOF mass spectrometry (Fig. S5, S8, and S11, ESI†), elemental analysis, attenuated total reflection Fourier-transform IR (ATR-FTIR) (Fig. S12, ESI†), and single-crystal X-ray analysis. The chemical shifts of non-exchangeable aromatic protons on the outer phenyl rings revealed remarkable structural/electronic features of the current molecules. All aromatic proton chemical shifts for the new molecules are found to be downfield ($\Delta\delta_{Ar-H} \sim$ 0.4–0.8 ppm) with respect to those of the parent p-type **C_8-BTBT**. This is consistent with our original design rationales indicating reduced electron density (π-electron deficiency). However, the chemical shifts of the aromatic protons in the dicarbonyl derivative **D(C_7CO)-BTBT** are observed surprisingly further downfield as compared to those in the bis(dicyanovinylene) derivative **D(C_7CC(CN)$_2$)-BTBT** (δ_{Ar-H} = 7.6–8.1 ppm → 8.0–8.6 ppm) (Fig. 2). Since dicyanovinylene is a much stronger electron withdrawing unit than carbonyl, one would expect the opposite trend in chemical shifts as typically observed with previously developed molecular semiconductors.[52–54]

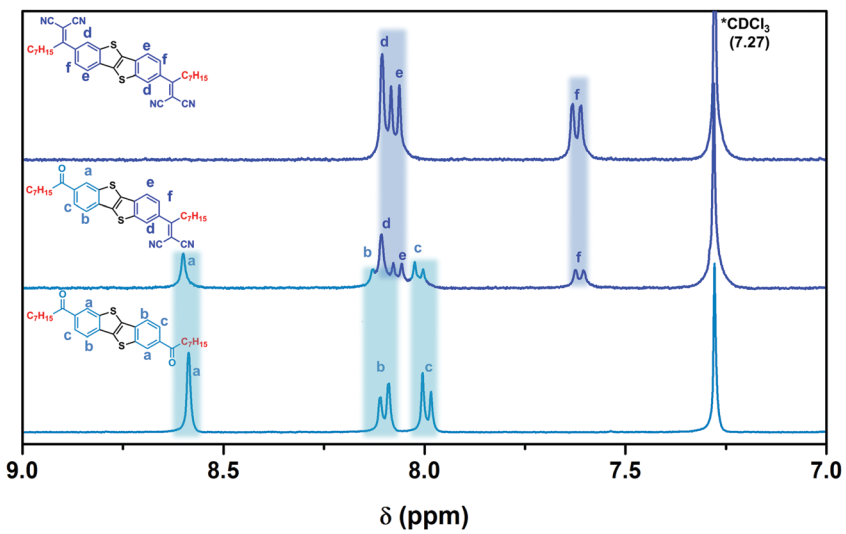

Fig. 2 The ^{1}H NMR spectra of **D(C_7CC(CN)$_2$)-BTBT** (top), **C_7CO-BTBT-CC(CN)$_2C_7$** (middle), and **D(C_7CO)-BTBT** (bottom) in $CDCl_3$ showing the chemical shifts of non-exchangeable aromatic protons "a–f".

The rationales behind this interesting electron-deficiency behavior upon carbonyl → dicyanovinylene conversion are twofold. Firstly, dicyanovinylene units adopt out-of-plane twisted conformations with respect to the BTBT π-system as evidenced by the single-crystal structure, DFT calculations, and photoluminescence studies, whereas carbonyls lie within the plane of the BTBT core, providing much stronger negative resonance (−*R*)/inductive (−*I*) effects. Secondly, the cyano groups (–CN) in the twisted dicyanovinylene unit exert shielding effects on nearby aromatic protons "d and f". A similar shielding effect was evident also on aliphatic β-protons – but not on α-protons due to geometrical restraints – in **D(C$_7$CC(CN)$_2$)-BTBT** as compared to **D(C$_7$CO)-BTBT** ($\delta_{\text{aliphatic }\beta\text{-H}}$: ~1.8 ppm → ~1.3 ppm). On the other hand, when **D(C$_7$CO)-BTBT** is compared with our previously developed **D(Ph$_F$CO)-BTBT**, minimum differences are observed in the ^{1}H NMR spectra, which reveals that the electronic effects of –C$_7$H$_{15}$ *vs.* –Ph$_F$ substituents – although they have completely different electron deficiencies and π-densities – have a minimum impact on the BTBT π-system. This is also supported by theoretically and experimentally determined frontier molecular orbitals of these two molecules that showed very similar energetics/wave functions (*vide infra*). The protons on each outer phenyl ring in unsymmetrical **C$_7$CO-BTBT-CC(CN)$_2$C$_7$** are independently found to follow the specific chemical shift patterns of carbonyl and dicyanovinylene functionalized aromatic units (middle ^{1}H NMR spectrum in Fig. 2). This reveals that there is minimal π-electronic interaction across the functionalized BTBT π-system, avoiding the formation of a new set of chemical shifts. This is most likely the direct result of the phene-like electronic structure of the BTBT π-system and it is further evidenced by electrochemical characterization (*vide infra*). To the best of our knowledge, this is the first time that fully separated electronic behaviors are observed for outer phenylenes in a diacene-fused thienothiophene π-system.

Thermal characterization was carried out by thermogravimetric analysis (TGA) and differential scanning calorimetry (DSC) under a nitrogen atmosphere and the data are presented in Table 1. As shown in Fig. 3A, the current compounds exhibit high thermolysis onset temperatures (T_{onset}, corresponding to 5% weight loss) of >300 °C, and dicyanovinylene functionalization was found to significantly increase the thermal stability (T_{onset} = 305 °C for **D(C$_7$CO)-BTBT** *vs.* T_{onset} = 375 °C for **D(C$_7$CC(CN)$_2$)-BTBT** and **C$_7$CO-BTBT-CC(CN)$_2$C$_7$**). **D(C$_7$CO)-BTBT**, **C$_7$CO-BTBT-CC(CN)$_2$C$_7$**, and **D(C$_7$CC(CN)$_2$)-BTBT** show major endothermic thermal transitions at 266 °C (26.9 J g^{-1}), 103 °C (28.4 J g^{-1}), and 212 °C (75.7 J g^{-1}), respectively, with the corresponding exothermic peaks at 265 °C (25.7 J g^{-1}), 61 °C (30.9 J g^{-1}), and 108 °C (77.0 J g^{-1}), respectively. These transitions are attributed to the melting (T_{mp}: 265–266 °C, 102–103 °C, and 211–212 °C, respectively) and crystallization processes as observed by conventional melting point measurements. Interestingly, in contrast to the increased melting point (ΔT_{mp} > 100 °C) upon dicyanovinylene functionalization on formerly reported carbonyl-functionalized molecular semiconductors,[53] the melting point of dicyanovinylene-functionalized **D(C$_7$CC(CN)$_2$)-BTBT** is found to be considerably lower (ΔT_{mp} = −54 °C) than that of carbonyl-functionalized **D(C$_7$CO)-BTBT**. Solid-state structural analysis (*vide infra*) reveals that although the carbonyls in **D(C$_7$CO)-BTBT** are completely in the BTBT π-plane (θ_{torsion} = 4.17° for BTBT/C=O) leading to the formation of a "layer-by-layer" stacking motif with herringbone-like packing between "CO–BTBT–CO" units, the dicyanovinylenes in **D(C$_7$CC(CN)$_2$)-BTBT** are significantly twisted (θ_{dihedral} = 47.55° for BTBT/C=C(CN)$_2$) with respect to BTBT, hampering π-coplanarity. On the other hand, the much lower melting point (ΔT_{mp} = −109/−163 °C) observed for unsymmetrically functionalized **C$_7$CO-BTBT-CC(CN)$_2$C$_7$**, which would be expected to stay between those of symmetrically functionalized derivatives, points to considerably weakened cohesive forces in the solid state. This indicates that in the design of low LUMO BTBT molecules symmetrical functionalization is key to realize effective solid-state intermolecular interactions (*i.e.*, *cohesive energetics*) for both efficient charge transport and technologically relevant thermal behavior (*i.e.*, T_{mp} > 150–200 °C for device processing). Note that, for the same reason, single-crystal of solid **C$_7$CO-BTBT-CC(CN)$_2$C$_7$** with sufficient diffraction quality could not be obtained, while the other two molecules yield single-crystals (*vide infra*). The melting temperatures of symmetrically functionalized **D(C$_7$CO)-BTBT** and **D(C$_7$CC(CN)$_2$)-BTBT** are much higher than that of **C$_8$-BTBT** (T_{mp} = 129–130 °C)[46] having the same

Table 1 Summary of the thermal, optical absorption, electrochemical, and OFET semiconducting properties of compounds **D(C$_7$CO)-BTBT**, **C$_7$CO-BTBT-CC(CN)$_2$C$_7$**, and **D(C$_7$CC(CN)$_2$)-BTBT** and the corresponding estimated frontier molecular orbital energies

Compounds	T_{mp}[a] (°C)	T_{DSC}[b] (°C) heating(cooling)	T_{onset}[c] (°C)	$\lambda_{\text{max}}^{\text{sol}}$[d] (nm) ($E_g^{\text{opt}}$ (eV))	$\lambda_{\text{max}}^{\text{film}}$[e] (nm) ($E_g^{\text{opt}}$ (eV))	$E_{\text{red-1/2}}$[f] (V)	E_{LUMO}[g] (eV)	E_{HOMO}[g] (eV)	μ^h[h] (cm^2 V^{-1} s^{-1}) (V_{th} (V))	$I_{\text{on}}/I_{\text{off}}$[h]
D(C$_7$CO)-BTBT	265–266	169/219/266 (265/213/139)	305	380 (3.10)	413 (2.81)	−0.89	−3.51	−6.61	(p) 0.03 (−10 V)	10^4–10^5
C$_7$CO-BTBT-CC(CN)$_2$C$_7$	102–103	103 (61)	375	389 (2.90)	388 (2.82)	−0.95	−3.45	−6.35	Not active	Not active
D(C$_7$CC(CN)$_2$)-BTBT	211–212	169/212 (108)	375	400 (2.83)	421 (2.72)	−1.10	−3.30	−6.13	(n) 0.004 (+27 V)	10^6–10^7

[a] Measured by conventional melting point apparatus. [b] From DSC scans under nitrogen at a scan rate of 10 °C min^{-1}. [c] Onset decomposition temperature measured by TGA under nitrogen. [d] From optical absorption in dichloromethane; the optical band gap is estimated from the low energy band edge of the solution-based UV-vis absorption spectrum. [e] From optical absorption as a spin-coated film on glass; the optical band gap is estimated from the low energy band edge of the film UV-vis absorption spectrum. [f] 0.1 M $Bu_4N^+PF_6^-$ in dichloromethane (*vs.* Ag/AgCl) at a scan rate of 50 mV s^{-1}. [g] Estimated from the equations $E_{\text{LUMO}} = -4.40\text{ eV} - E_{\text{red-1/2}}$ and $E_g = E_{\text{LUMO}} - E_{\text{HOMO}}$. [h] Majority charge carrier types, electron/hole mobilities, threshold voltages, and current on/off ratios from top-contact/bottom-gate OFET devices of n^{++}-Si/SiO$_2$ (200 nm)/HMDS/vapor-deposited (at 70 °C) semiconductor (30 nm)/LiF (for n-type only)–Au (50 nm).

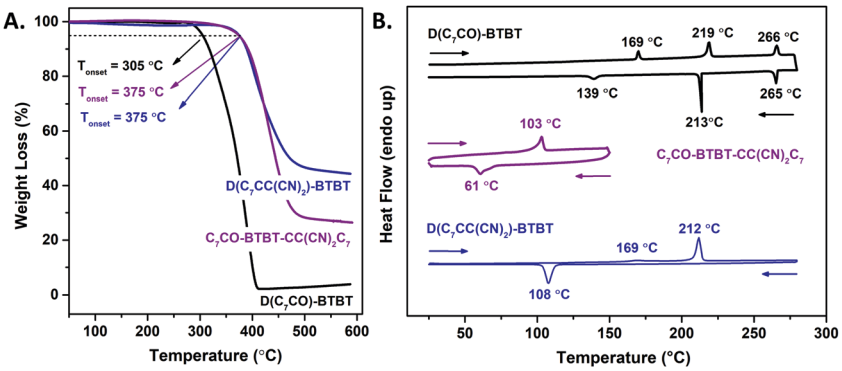

Fig. 3 (A) Thermogravimetric analysis (TGA) and (B) differential scanning calorimetry (DSC) measurement curves of **D(C$_7$CO)-BTBT**, **C$_7$CO-BTBT-CC(CN)$_2$C$_7$**, and **D(C$_7$CC(CN)$_2$)-BTBT** at a temperature ramp of 10 °C min^{-1} under N_2.

alkyl chain length, which could be attributed to the presence of polar functional groups and a slightly more extended π-framework, leading to enhanced intermolecular cohesion. For **D(C$_7$CO)-BTBT** and **D(C$_7$CC(CN)$_2$)-BTBT**), additional thermal peaks at 169 (16.2 J g^{-1})/219 °C (51.3 J g^{-1}) and 169 °C (4.6 J g^{-1}), respectively, were observed prior to the highest temperature transition to the isotropic liquid phase. These thermal transitions could be attributed to the formation of liquid-crystal (LC) phase(s) as previously observed for BTBT derivatives with similar alkyl chains,[55] and it reflects the presence of flexible heptyl chains at the molecular ends. Note that our previously developed n-channel BTBT semiconductor **D(Ph$_F$CO)-BTBT** did not exhibit any thermal transition prior to melting as a result of having rigid perfluorophenyl (–Ph$_F$) rings.

Single-crystal structure and intermolecular interactions

Single-crystals of **D(C$_7$CO)-BTBT** and **D(C$_7$CC(CN)$_2$)-BTBT** were grown as clear yellow needles by slow diffusion of methanol into chloroform solution and as red plates by slow evaporation of chloroform solution, respectively. The crystal structures determined by single-crystal X-ray diffraction are shown in Fig. 4, and the crystallographic data are provided in Table S1 (ESI†). The crystal structures and packing properties of the current compounds are discussed in comparison to our recently developed high mobility n-type semiconductor **D(Ph$_F$CO)-BTBT**[34] in order to gain complete insight into this new class of functionalized low LUMO BTBTs. Although the conjugated backbone of the BTBT unit in **D(C$_7$CO)-BTBT** and **D(C$_7$CC(CN)$_2$)-BTBT** is highly coplanar with no ring-to-ring twist angles ($\theta_{Ar–Ar} \sim 0°$; Ar is phenyl or thienyl) as in **D(Ph$_F$CO)-BTBT** and other (un)substituted BTBT molecular π-skeletons,[34,46,56] the three-dimensional configurations of the functional groups and the substituents are found to be quite different. While a small torsion angle of 4.17° is measured between the carbonyls and the BTBT π-unit (C6–C1(phenylene)–C=O) in **D(C$_7$CO)-BTBT** leading to a substantially coplanar molecular backbone with extended π-conjugation, the dicyanovinylenes in **D(C$_7$CC(CN)$_2$)-BTBT** are found to be twisted ($\theta_{torsion}$ = 44.92° for C6–C1(phenylene)–C11–C10(dicyanovinylene) and $\theta_{dihedral}$ = 47.55° for BTBT/C=C(CN)$_2$) out of the BTBT π-plane. These twist angles for the dicyanovinylene units are slightly higher than the ~40° maximum value beyond which electronic communication weakens to support intramolecular π-conjugation.[53,57] Both of these solid-state conformations are consistent with the DFT-calculated molecular structures, which exhibit ~0°/~44° torsion/dihedral angles between BTBT and carbonyl/dicyanovinylene functionalities (Fig. S13, ESI†). The solid-state molecular conformation of **D(C$_7$CO)-BTBT** matches well with that of our recently reported dicarbonyl BTBT molecule **D(Ph$_F$CO)-BTBT** ($\theta_{torsion}$ = 1.87° for C8–C7(phenylene)–C=O),[34] suggesting that 2,7-carbonyls, regardless of the substituents (heptyl *vs.* pentafluorophenyl), tend to stay within the BTBT π-plane, yielding π-extended electron-deficient BTBTs. Although alkyl substitution, and thus the presence of α-methylene, appears not to be detrimental to functional group coplanarity when used with carbonyl, it is found to cause twists with dicyanovinylene functionalities. The intramolecular twists in **D(C$_7$CC(CN)$_2$)-BTBT** most likely originate from an interplay of C6–H6(phenylene)/C8≡N1(dicyanovinylene) and C2–H2(phenylene)/C12–H12A-B-(α-methylene) steric interactions. Theoretical modelling on a hypothetical unsubstituted dicyanovinylene-functionalized BTBT molecule **D(HCC(CN)$_2$)-BTBT** (Fig. S14, ESI†), although it would be a relatively difficult synthetic target with low solubility, reveals that dicyanovinylene groups could be effectively within the BTBT π-plane upon removal of the alkyl substituents. This provides valuable insight into future design of π-extended low LUMO DAcTTs.

D(C$_7$CO)-BTBT crystallizes in the monoclinic space group *C*2/*c* showing alternating layers of conductive π-segments (CO–BTBT–CO) and insulating alkyl substituents (–C$_7$H$_{15}$) along the crystallographic *a*-axis (Fig. 4A). The heptyl chains at the molecular termini display a fully extended all-trans conformation, and they are perfectly aligned along the molecular long-axis allowing for the formation of pure hydrocarbon layers along the *a*-axis. **D(C$_7$CO)-BTBT** molecules display a slipped stacked packing arrangement along the *c*-axis using short intermolecular S···S contacts (a = 3.43 Å < r_{vdW} (S) + r_{vdW} (S) = 3.60 Å).[58] Along the *b*, *c*-axes, herringbone-like molecular packing was identified with major intermolecular interactions of C–H(phenyl)···π(phenyl) (b, c, e = 3.57, 2.78, 3.27 Å), S···π(thienyl) (d = 3.22 Å), and C=O(δ^-)···C(δ^+)=O (f = 3.52 Å). When the crystal properties for **D(C$_7$CO)-BTBT** and **D(Ph$_F$CO)-BTBT**[34] (Fig. 4C) are compared, although the packing motifs and intermolecular interactions are found to be very similar,

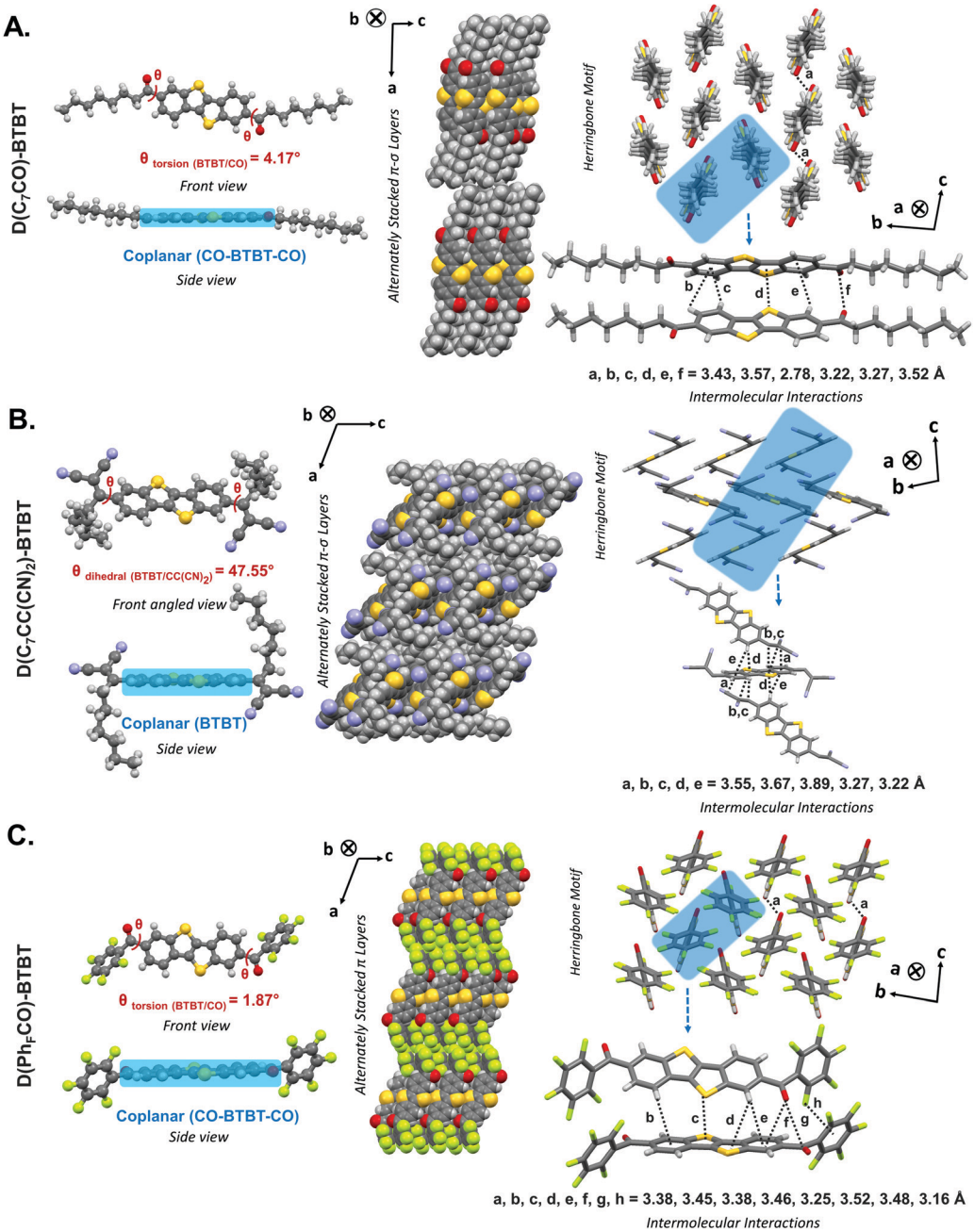

Fig. 4 Ball and stick drawings of the molecular structures showing the corresponding torsion/dihedral angles (between the BTBT π-core and functional groups) and π-backbone coplanarity, perspective views of the molecular arrangements and packings along the crystallographic *a*, *c*-axes and *b*, *c*-axes showing the alternately stacked layers and the herringbone motifs/packing, and the intermolecular interactions for **D(C$_7$CO)-BTBT**. (A) (*a* = S···S; *b*, *c*, *e* = C–H(phenyl)···π(phenyl); *d* = S···π(thienyl); *f* = C═O(δ^-)···C(δ^+)═O), **D(C$_7$CC(CN)$_2$)-BTBT**. (B) (*a* = N≡C···π(phenyl); *b*, *c* = C═C(dicyanovinylene)···π(thienyl); *d*, *e* = C–H(phenyl)···π(thienyl/phenyl)), and our previously reported n-type semiconductor **D(Ph$_F$CO)-BTBT**.[34] (C) (*a* = S···S; *b*, *e* = C–H(phenyl)···π(phenyl); *c* = S···π(thienyl); *d* = C–H(phenyl)···π(thienyl); *f* = C═O···π(phenyl); *g* = C═O(δ^-)···C(δ^+)═O; *h* = F···π(pentafluorophenyl)). Heptyl chains are omitted for clarity in the herringbone motif/packing in panel B.

the specific herringbone-like arrangements are found to show a clear distinction with regard to the molecular offsets along the long-axis directions. While **D(Ph$_F$CO)-BTBT** shows a molecular offset of half an aromatic unit resulting in strong three dimensional BTBT···carbonyl intermolecular interactions, **D(C$_7$CO)-BTBT** molecules are found to adopt perfectly matched (*i.e.*, no molecular offset) herringbone packing without BTBT···carbonyl interactions. **D(C$_7$CC(CN)$_2$)-BTBT** crystallizes in the monoclinic space group $P2_1/c$. Although the heptyl chains at the molecular termini are not in their fully extended all-*trans* conformation, and they are found to align towards the top and bottom of the BTBT π-system, **D(C$_7$CC(CN)$_2$)-BTBT** crystals show alternating layers of conductive π-segments ((CN)$_2$C═C–BTBT–C═C(CN)$_2$) and insulating alkyl substituents (–C$_7$H$_{15}$) along the crystallographic

a-axis (Fig. 4B). However, the herringbone packing along the *b*, *c*-axes becomes more complicated due to its twisted molecular structure. Each **D(C$_7$CC(CN)$_2$)-BTBT** molecule is found to interact with four other molecules in three dimensions (only two are shown in Fig. 4B to avoid visual crowding) to form intermolecular N≡C···π(phenyl) (*a* = 3.55 Å), C=C(dicyanovinylene)···π(thienyl) (*b*, *c* = 3.67, 3.89 Å), and C–H(phenyl)···π(thienyl/phenyl) (*d*, *e* = 3.27, 3.22 Å) contacts. Different from the carbonyl-functionalized BTBT derivatives, **D(C$_7$CC(CN)$_2$)-BTBT** molecules did not exhibit any S···S contacts; instead short intermolecular N···H contacts (2.52 Å < r_{vdW} (N) + r_{vdW} (H) = 2.75 Å) are identified.[58] Similar to our previously reported n-type **D(Ph$_F$CO)-BTBT**, strong BTBT···dicyanovinylene intermolecular interactions are identified in solid-state **D(C$_7$CC(CN)$_2$)-BTBT**. The electron withdrawing carbonyl and dicyanovinylene functionalities in **D(Ph$_F$CO)-BTBT** and **D(C$_7$CC(CN)$_2$)-BTBT** electronically interact with the BTBT π-system, contributing to the formation of three dimensional electron transporting π-electronic structures, which enables efficient n-channel transport in the solid-state (*vide infra*). In contrast, the carbonyls in **D(C$_7$CO)-BTBT** do not show the same type of π-interaction, and the BTBT units interact only with themselves as typically seen in previously reported p-type DAcTTs,[31,46] resulting in hole transport (*vide infra*) despite its low LUMO. For both molecules, the observed herringbone-like packing and short intermolecular interactions involving π-conjugated units are expected to enable two-dimensional charge transport when crystalline domains are properly oriented in the corresponding semiconductor thin films.

Photophysical and electrochemical properties

In order to reveal the effects of carbonyl *vs.* dicyanovinylene functionalization and alkyl *vs.* pentafluorophenyl substitutions on the optoelectronic characteristics of the BTBT π-system, the current molecules are studied by UV-vis absorption and photoluminescence spectroscopies, and cyclic voltammetry in dichloromethane solutions (1.0×10^{-5} M) and as thin-films. The photophysical and electrochemical data are presented in Table 1. As shown in Fig. 5A, typical vibronic features (~1400–1600/3000–3100 cm^{-1} for aromatic C=C/C–H bond stretches) of a fused heteroacene π-system are observed for all compounds with bathochromically shifted low-energy absorption maxima (λ_{max} = 380 nm for **D(C$_7$CO)-BTBT**, λ_{max} = 389 nm for **C$_7$CO-BTBT-C(CCN$_2$)C$_7$**, and λ_{max} = 400 nm for **D(C$_7$CC(CN)$_2$)-BTBT**) and onsets (λ_{onset} = 400 nm for **D(C$_7$CO)-BTBT**, λ_{onset} = 427 nm for **C$_7$CO-BTBT-CC(CN)$_2$C$_7$**, and λ_{onset} = 438 nm for **D(C$_7$CC(CN)$_2$)-BTBT**) with respect to the non-functionalized alkyl-substituted derivative **C$_8$-BTBT** (λ_{max} = 330 nm/λ_{onset} = 340 nm, Fig. S15, ESI†). The optical band gaps are estimated to be 3.10 eV for **D(C$_7$CO)-BTBT**, 2.90 eV for **C$_7$CO-BTBT-CC(CN)$_2$C$_7$**, and 2.83 eV for **D(C$_7$CC(CN)$_2$)-BTBT**, which are

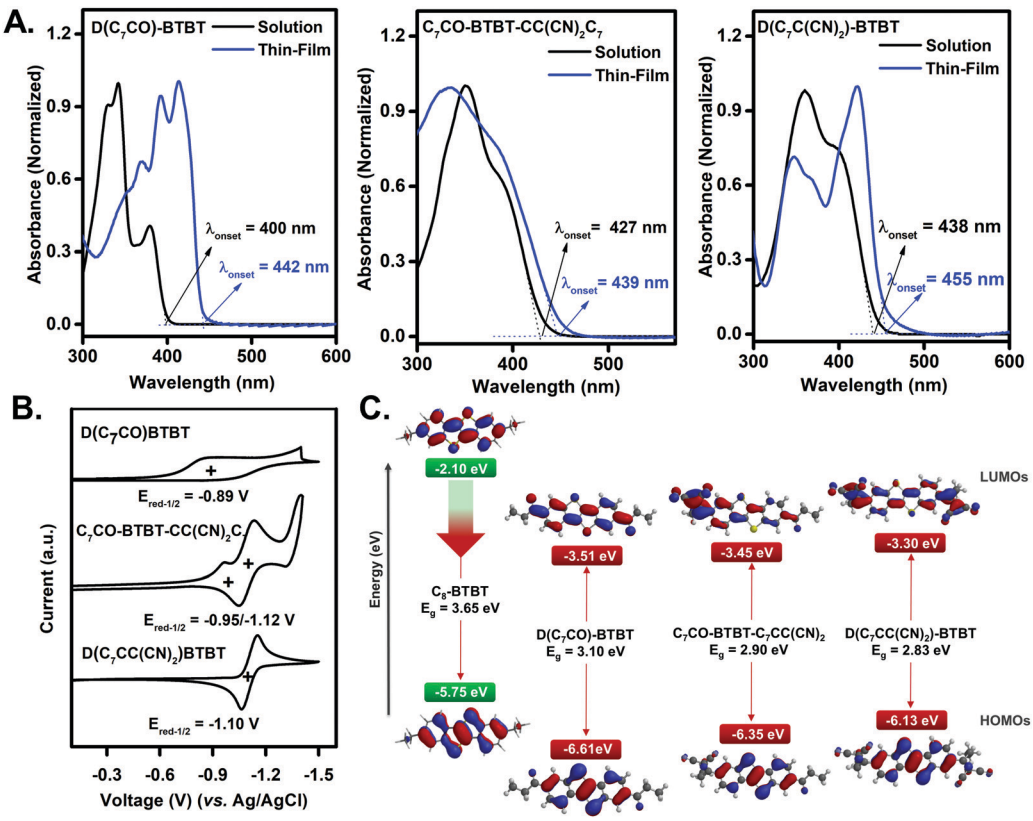

Fig. 5 (A) Optical absorption spectra (in dichloromethane and as spin-coated thin films), (B) cyclic voltammograms *vs.* Ag/AgCl (3.0 M NaCl) (in 0.1 M $Bu_4N^+PF_6^-$ dichloromethane, scan rate = 50 mV s^{-1}), and (C) experimentally determined frontier molecular orbital energies along with topographical orbital representations (DFT/B3LYP/6-31G**) for **D(C$_7$CO)-BTBT**, **C$_7$CO-BTBT-CC(CN)$_2$C$_7$**, and **D(C$_7$CC(CN)$_2$)-BTBT**.

significantly smaller than that of **C_8-BTBT** (E_g^{opt} = 3.65 eV), reflecting the electronic (negative resonance ($-R$)/inductive ($-I$)) and π-extension effects of carbonyl/dicyanovinylene functionalities. The conversion of the carbonyl functionality into dicyanovinylene gradually decreases the optical band gap of the BTBT π-system (λ_{onset} = 400 nm → 427 nm → 438 nm). As shown in Fig. S16 (ESI†), upon changing the solvent media from low to medium polarity (hexane ($f(\varepsilon,n)$ = 0.001) → dichloromethane ($f(\varepsilon,n)$ = 0.217), the low-energy absorption maxima and onsets for all three molecules show bathochromic shifts, suggesting that the Franck–Condon excited state ($S_{1(FC)(\pi-\pi^*)}$) has a higher dipole than the ground state (S_0). This could be attributed to the presence of electron withdrawing end functionalities adjacent to a relatively π-electron rich BTBT. Note that the most notable red-shift (~30 nm) was observed with **D(C_7CC(CN)$_2$)-BTBT** having two strongly electron withdrawing dicyanovinylene end units. Surprisingly, when the solvent polarity is further increased (*N*,*N*′-dimethylformamide (DMF) ($f(\varepsilon,n)$ = 0.276) and dimethyl sulfoxide (DMSO) ($f(\varepsilon,n)$ = 0.263)), the molecules having dicyanovinylene unit(s) (*i.e.*, **C_7CO-BTBT-CC(CN)$_2$C$_7$** and **D(C_7CC(CN)$_2$)-BTBT**) show completely opposite spectral shifts to smaller wavelengths ($\Delta\lambda_{max}$ ~ −20 to 60 nm). The absorption maximum for **D(C_7CC(CN)$_2$)-BTBT** in DMSO is very similar to those of non-functionalized BTBT compounds.[31,46] This unexpected hypsochromic shift in highly polar medium seems to originate from reduced π-delocalization on the molecular backbone, most likely through intramolecular BTBT-dicyanovinylene rotations. In contrast, coplanar dicarbonyl compound **D(C_7CO)-BTBT** did not exhibit any spectral shift upon going to highly polar medium; instead, an n–π* transition becomes apparent at ~424 nm. A similar n–π* transition was also observed for **C_7CO-BTBT-CC(CN)$_2$C$_7$** in DMF at ~460 nm. When going from solution to the solid-state, although unsymmetrical **C_7CO-BTBT-CC(CN)$_2$C$_7$** shows a slightly broadened spectrum with a small bathochromic shift ($\Delta\lambda_{onset}$ ~ 10 nm), **D(C_7CO)-BTBT** and **D(C_7CC(CN)$_2$)-BTBT** exhibit obvious J-aggregate like spectral changes with large bathochromic shifts ($\Delta\lambda_{max}$ ~ 60–70 nm/$\Delta\lambda_{onset}$ ~20–45 nm). This indicates significantly enhanced intermolecular interactions (cohesive energetics) in the solid-state of these two molecules as compared to **C_7CO-BTBT-CC(CN)$_2$C$_7$**, which is consistent with the measured melting temperatures (*vide supra*).

As shown in Fig. 5B, the electrochemical characterization of the current BTBT molecules shows clear (quasi)reversible first reduction peaks (*vs.* Ag/AgCl) at −0.89 V for **D(C_7CO)-BTBT**, −0.95 V for **C_7CO-BTBT-CC(CN)$_2$C$_7$**, and −1.10 V for **D(C_7CC(CN)$_2$)-BTBT**. Considering that alkyl substituted non-functionalized **C_8-BTBT** shows only an oxidation peak at 1.35 V (*vs.* Ag/AgCl) (Fig. S15 – inset, ESI†), the electron withdrawing carbonyl and dicyanovinylene functionalization at BTBT's 2,7-positions clearly increase the π-electron deficiency and enable the reduction process. The unsymmetrically functionalized **C_7CO-BTBT-CC(CN)$_2$C$_7$** shows two consecutive reductions at −0.95 V/−1.12 V, and each reduction alone follows the electrochemical behavior of carbonyl- and dicyanovinylene-functionalized BTBT π-units. The LUMO energy levels of the current molecules are estimated to be −3.51 eV, −3.45 eV, and −3.30 eV, respectively, which are in the range of those (−2.9 eV to −4.3 eV) previously reported for n-channel organic semiconductors.[36,37] These LUMOs are greatly stabilized (ΔE_{LUMO} = −1.2–1.4 eV) with respect to that of **C_8-BTBT** (E_{LUMO} = −2.10 eV), pointing out strong negative resonance ($-R$)/inductive ($-I$) effects of the carbonyl/dicyanovinylene units at the 2,7-positions. Also, highly delocalized LUMOs calculated over the entire molecular π-backbones could be advantageous for electron transport. As compared with our recently developed **D(Ph_FCO)-BTBT** having pentafluorophenyl units, the slightly higher (~0.13 eV) LUMO estimated for **D(C_7CO)-BTBT** is ascribed to the electron-donating ability of the heptyl chains. Interestingly, the LUMO level was found to increase upon carbonyl-to-dicyanovinylene conversions in the order of **D(C_7CO)-BTBT → C_7CO-BTBT-CC(CN)$_2$C$_7$ → D(C_7CC(CN)$_2$)-BTBT**. Considering that dicyanovinylene has a much stronger electron withdrawing ability typically leading to a LUMO stabilization of ~0.5–1.0 eV with respect to its carbonyl-functionalized counterpart,[6,53,59] this rather surprising frontier molecular orbital energy trend implies deteriorated π-conjugation between dicyanovinylene and BTBT units in solution. The solid-state molecular structure of **D(C_7CC(CN)$_2$)-BTBT** confirms the formation of large intramolecular twists upon dicyanovinylene functionalization ($\theta_{dihedral}$ = 47.55° for BTBT/C═C(CN)$_2$), which is very likely to increase in solution going beyond the limiting dihedral angle (≫40°) to support efficient intramolecular π-overlap.[57,60] The theoretical calculations on **D(C_7CC(CN)$_2$)-BTBT** conformations with varied dihedral angles (Fig. S17, ESI†) indeed show that the degree of LUMO destabilization becomes much faster at higher dihedral angles of >45° (ΔE_{LUMO} ~ 0.85 eV for $\theta_{dihedral}$ = 45° → 90° *vs.* ΔE_{LUMO} ~ 0.3 eV for $\theta_{dihedral}$ = 0° → 45°), and the corresponding wave functions eventually get localized on the dicyanovinylenes.

The steady-state fluorescence and time-resolved photoluminescence decays (λ_{exc} = 375 nm and 200 ps pulse width) of **D(C_7CO)-BTBT** and **D(C_7CC(CN)$_2$)-BTBT** were studied in order to better understand the optoelectronic effects of in-plane carbonyls *vs.* twisted dicyanovinylenes. As shown in Fig. 6A, for the same concentrations (1.0×10^{-5} M) in dichloromethane, **D(C_7CC(CN)$_2$)-BTBT** showed a much weaker fluorescence peak with decreased (10×) quantum yield (Φ_{PL} = 0.1 → 0.01) and increased Stokes shift ($\Delta\lambda_{Stokes\ shift}$ ~ 60 nm) in comparison to **D(C_7CO)-BTBT**. Similarly, time-resolved photoluminescence decay measurements indicated a faster decay profile for **D(C_7CC(CN)$_2$)-BTBT** with a lifetime of 0.19 ns (τ_1 = 0.40 ns for **D(C_7CO)-BTBT**). Therefore, it is apparent that highly twisted dicyanovinylene units adjacent to the BTBT π-system induce significant non-radiative relaxation of the excited state (fluorescence quenching) in solution as compared to in-plane carbonyls. To better understand the origin of the non-radiative decay, PL properties for **D(C_7CC(CN)$_2$)-BTBT** were measured in a solvent system with similar polarities but different viscosities (*i.e.*, methanol (0.54 cP) and ethylene glycol (16.1 cP)).[61] As shown in Fig. 6B, the photoluminescence intensity was found to be enhanced (~4×) and the corresponding PL decay profile became slower (τ_1 = 0.17 ns → 0.39 ns) in the higher viscosity medium, which implies that BTBT/dicyanovinylene

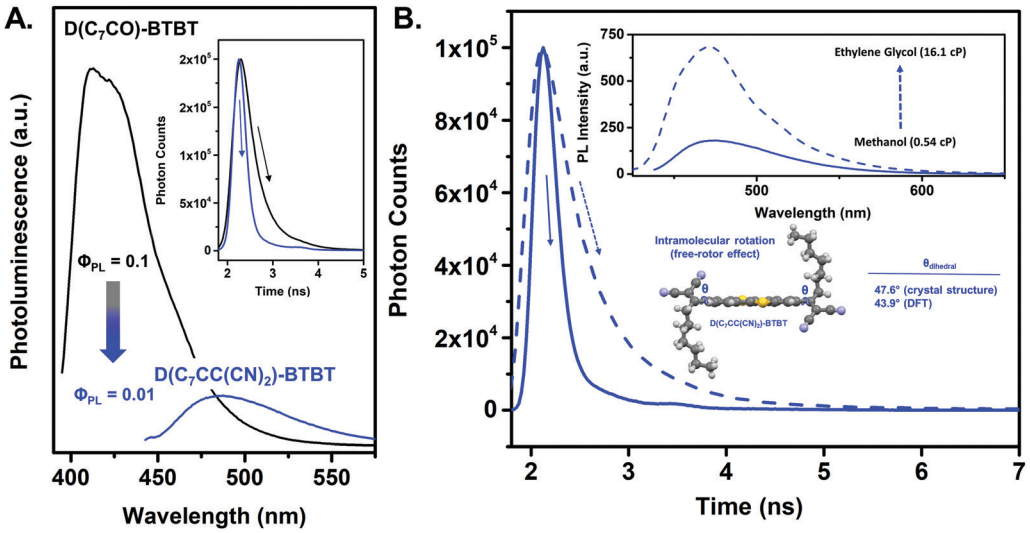

Fig. 6 (A) Photoluminescence spectra of **D(C$_7$CO)-BTBT** (λ_{exc} = 385 nm) and **D(C$_7$CC(CN)$_2$)-BTBT** (λ_{exc} = 405 nm) in dichloromethane (1.0×10^{-5} M). The inset shows the transient photoluminescence decay profiles (λ_{exc} = 375 nm and 200 ps pulse width) measured at 410 nm and 483 nm for **D(C$_7$CO)-BTBT** and **D(C$_7$CC(CN)$_2$)-BTBT**, respectively, in dichloromethane (10^{-5} M) under a nitrogen atmosphere. (B) The transient photoluminescence decay profiles measured at 483 nm for **D(C$_7$CC(CN)$_2$)-BTBT** (λ_{exc} = 375 nm and 200 ps pulse width) in methanol (solid) and ethylene glycol (dashed) solutions (10^{-5} M) under a nitrogen atmosphere. The inset shows the solvent viscosity-dependent (methanol (0.54 cP) and ethylene glycol (16.1 cP)) photoluminescence spectra for **D(C$_7$CC(CN)$_2$)-BTBT**.

rotations are more constrained in the higher viscosity medium to partially deactivate non-radiative decay.[62] Similarly, going into the solid-state, the PL quantum yield of **D(C$_7$CC(CN)$_2$)-BTBT** was found to dramatically increase (Φ_{PL} = 0.01 → 0.11). Based on these results and considering that solvent polarity-dependent PL (Fig. S18, ESI†) does not reveal charge-transfer excited state formation, it is clear that the highly twisted dicyanovinylenes in **D(C$_7$CC(CN)$_2$)-BTBT** activate non-radiative decay channels in solution through intramolecular rotations (free-rotor effect). Similar free-rotor effects have been observed in previously reported aryl-dicyanovinylene molecules.[63,64] BTBT-dicyanovinylene compounds, especially when combined with their optoelectronic and semiconducting properties, could constitute a novel rotor family for various molecular sensing applications. Here, it's noteworthy that high frequency vibrations (loose-bolt effect) could also be somewhat contributing to the observed non-radiative decay in the dicyanovinylene units.[65]

Thin-film microstructure/morphology and field-effect transistor characterization

The charge transport characteristics of **D(C$_7$CO)-BTBT** and **D(C$_7$CC(CN)$_2$)-BTBT** were studied in top-contact/bottom-gate (TC/BG) OFETs by thermally evaporating semiconductor thin films (30 nm) onto temperature controlled (25 and 70 °C) n^{++}-Si/SiO_2 (200 nm)/HMDS substrates. Source and drain electrodes (Au (50 nm) for p-channel and LiF (1 nm)/Au (50 nm) for n-channel) were defined *via* thermal evaporation. Prior to the charge-transport measurements, the morphology and microstructure of the BTBT thin films were studied by atomic force microscopy (AFM) and grazing-incidence X-ray diffraction (GIXD). As shown in Fig. 7A and B, the thin film surface morphologies of both molecules show well-interconnected crystalline domains, and clear transitions from relatively small (~150–200 nm) granular shaped grains to micron-sized (~0.6–2.0 μm) 2D plate-like grains of terraced islands along the substrate plane were observed upon increasing the deposition temperature. The out-of-plane θ–2θ GIXD analysis shows major diffraction peaks at $2\theta = 5.80°/8.68°$ for **D(C$_7$CO)-BTBT** and at $2\theta = 5.21°$ for **D(C$_7$CC(CN)$_2$)-BTBT** (Fig. 7C), which correlates perfectly with the single-crystal lattice planes of (400)/(600) and (100), respectively, based on the corresponding powder pattern simulations (Fig. S19, ESI†). Using the single crystal structural data, the Bravais–Friedel–Donnay–Harker (BFDH) theoretical crystal morphologies were predicted for both semiconductors, which confirm the growth of 2D plate-like crystalline domains on the substrate plane and along the (400)/(600) (for **D(C$_7$CO)-BTBT**) and (100) (for **D(C$_7$CC(CN)$_2$)-BTBT**) lattice planes (Fig. 7D). This indicates great agreement between the single-crystal structures and thin film microstructures/morphologies, and it suggests that the in-plane packing motifs of the observed 2D plate-like crystalline grains in the thin film phase have herringbone-like intermolecular interactions similar to the corresponding single-crystal structures. Interestingly, the **D(C$_7$CO)-BTBT** thin film deposited at room temperature shows a clear high-angle diffraction peak at $2\theta = 23.09°$ that corresponds to (020) lattice planes formed with entirely face-on oriented molecules (Fig. S20, ESI†). This facile control between face-on and edge-on orientations with deposition temperature is a unique feature to study charge transport in various optoelectronic devices. The face-on molecular arrangement could be quite useful for the fabrication of functional semiconductor layers in which vertical charge transport is required along with a low LUMO and wide optical band gap (*e.g.*, passivation layer on metal oxide thin-film electronics, photodiodes, and organic photovoltaics).[66–72]

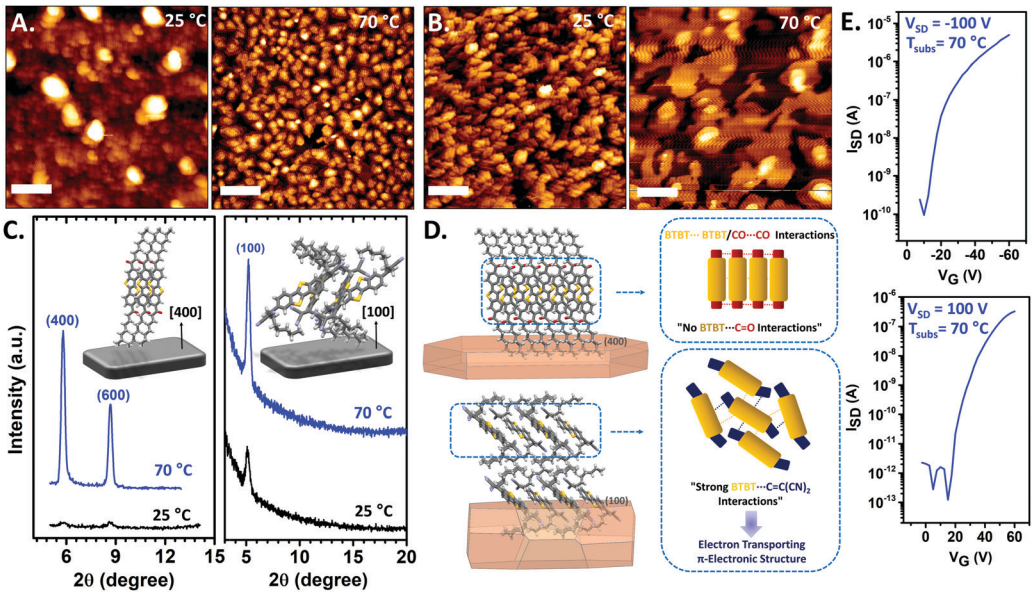

Fig. 7 Tapping mode atomic force microscopy (AFM) topographic images and grazing incidence X-ray diffraction (GIXRD) scans for **D(C$_7$CO)-BTBT** (A and C – left) and **D(C$_7$CC(CN)$_2$)-BTBT** (B and C – right) thin films deposited on n^{++}-Si/SiO$_2$ (200 nm)/HMDS at 25 °C and 70 °C, and the molecular arrangements in the out-of-plane directions. The scale bar denotes 1 μm. (D) The Bravais–Friedel–Donnay–Harker (BFDH) theoretical crystal morphologies, the views of the packing arrangements in the 2D plate-like crystalline grains, and the corresponding lattice planes. (E) Transfer (V_{SD} = −100 V for **D(C$_7$CO)-BTBT** and V_{SD} = 100 V for **D(C$_7$CC(CN)$_2$)-BTBT**) characteristics for the n^{++}-Si/SiO$_2$ (200 nm)/HMDS/**D(C$_7$CO)-BTBT** (30 nm)/Au (50 nm) (top) and n^{++}-Si/SiO$_2$ (200 nm)/HMDS/**D(C$_7$CC(CN)$_2$)-BTBT** (30 nm)/LiF (1 nm)/Au (50 nm) (bottom) OFET devices fabricated at a substrate temperature of 70 °C.

The electrical characteristics of the OFETs fabricated at a substrate temperature of 70 °C were measured under both positive and negative gate biases to reveal the majority charge carriers and semiconducting performances. Here, we note that we were not able to measure the charge transport characteristics of these molecules from their spin-coated/drop-cast thin films due to undesirable film formation. As shown in Fig. 7E, **D(C$_7$CO)-BTBT** and **D(C$_7$CC(CN)$_2$)-BTBT** exhibit p-type and n-type semiconducting behaviors with appreciable hole and electron mobilities of 0.03 cm^2 V^{-1} s^{-1} (I_{on}/I_{off} = 10^4–10^5 and V_{th} = −10 V) and 0.004 cm^2 V^{-1} s^{-1} (I_{on}/I_{off} = 10^6–10^7 and V_{th} = +27 V), respectively. Following our initial report on high electron mobility **D(Ph$_F$CO)-BTBT**, **D(C$_7$CC(CN)$_2$)-BTBT** now becomes a novel and rare n-type DAcTT semiconductor, which contributes to the development of an electron transporting DAcTT library by not only adding new functionalities (*i.e.*, introducing solubility and using new π-extended functional groups) but also elucidating "structure–molecular properties–semiconductivity" relationships. In this new family of functionalized low LUMO BTBTs, from a molecular design perspective, the observed trends in the majority charge carriers (p-type for **D(C$_7$CO)-BTBT** *vs.* n-type for **D(C$_7$CC(CN)$_2$)-BTBT**/**D(Ph$_F$CO)-BTBT**) could not be explained simply by the frontier molecular orbital energies/topographies as is the typical approach in the field of organic optoelectronics.[4,73,74] The anomalies are: (i) for the carbonyl-functionalized BTBTs, although they share the common coplanar "CO–BTBT–CO" π-backbone leading to similar LUMO energies (∼−3.5 eV)/topographies (delocalized on the CO–BTBT–CO π-system), **D(C$_7$CO)-BTBT** behaves as p-type while **D(Ph$_F$CO)-BTBT** is an n-type semiconductor, (ii) for the alkyl substituted BTBTs, despite its lower LUMO energy (E_{LUMO} = −3.51 eV), **D(C$_7$CO)-BTBT** behaves as p-type while **D(C$_7$CC(CN)$_2$)-BTBT** is an n-type semiconductor, and (iii) considering that the substituents are not part of the LUMOs in functionalized low-LUMO BTBTs, how do they contribute to the observed majority charge carrier inversion? These findings strongly suggest that the low LUMO energies and π-delocalized LUMO topographies should be evaluated in combination with additional structural/optoelectronic parameters. Our detailed analysis has indeed revealed that the observed semiconducting behaviors reflect an interplay of two additional factors: (i) functional group contribution in the π-electronic structure along the charge transport direction and (ii) relative intramolecular reorganization energies for hole- *vs.* electron transport. Firstly, although all three BTBT semiconductors exhibit herringbone-like packing along the charge transport direction, a subtle packing difference, which is not obvious at first glance, is identified in the formation of π-electronic structures between n- and p-type semiconductors. In the herringbone motifs of n-type **D(C$_7$CC(CN)$_2$)-BTBT** and **D(Ph$_F$CO)-BTBT**, electron deficient carbonyl/dicyanovinylene functional groups continuously interact with the BTBT π-sytem (BTBT···carbonyl ∼ 3.5 Å/BTBT···dicyanovinylene ∼ 3.5–3.8 Å) in a three dimensional alternating fashion to form a π-electronic structure that is favorable for electron transport (Fig. 7D – bottom). However, in p-type **D(C$_7$CO)-BTBT**, a similar type of BTBT···carbonyl interactions was not present, and the BTBT π-units are found to interact only with themselves (Fig. 7D – top), as in non-functionalized p-type thienoacenes, which enables

a hole transporting π-electronic structure. Secondly, the relative intramolecular reorganization energies for hole *vs.* electron transport are found to be greatly affected by the substituents. As a key charge transport parameter, λ defines the intramolecular structural reorganization needed to accommodate a certain charge carrier type, and a smaller λ_e is typically desired for efficient electron transport.[75] Herein, we compare p-type **D(C_7CO)-BTBT** with n-type **D(Ph_FCO)-BTBT** because these molecules have the common charge transporting CO–BTBT–CO π-segment with similar π-electron deficiency, and any difference in the λs should be the direct result of substituent modification (alkyl *vs.* pentafluorophenyl). While the reorganization energy associated with the electron transfer in n-type **D(Ph_FCO)-BTBT** is smaller than that with the hole transfer (λ_e = 317 meV < λ_h = 360 meV), λ_e is calculated to be much larger than λ_h (355 meV ≫ 252 meV) in p-type **D(C_7CO)-BTBT**. These results are in great agreement with the observed majority charge carrier types. The effect of substituents on the λs has been demonstrated for different π-systems in former theoretical and experimental studies.[76–78] On the other hand, the larger λ_e calculated for the new n-type **D(C_7CC(CN)$_2$)-BTBT** as compared to **D(Ph_FCO)-BTBT** (λ_e = 509 meV ≫ 317 meV) might reflect the enhanced dihedral angle of the dicyanovinylenes to partly explain the observed lower electron mobility.[79] In our OFET studies, semiconductor thin films with proper surface coverage could not be achieved with unsymmetrical **C_7CO-BTBT-CC(CN)$_2$$C_7$**, which is probably due to unfavorably weak cohesive forces present in the solid-state of this molecule as discussed earlier.

Conclusions

In summary, a series of systematically functionalized [1]benzothieno[3,2-*b*][1]benzothiophene (BTBT)-based small molecules, **D(C_7CO)-BTBT**, **C_7CO-BTBT-CC(CN)$_2$$C_7$**, and **D($C_7$CC(CN)$_2$)-BTBT**, has been developed, which, when combined with our previously reported first n-type BTBT semiconductor **D(Ph_FCO)-BTBT**, gives the first molecular library of low LUMO DAcTTs. The new molecules exhibit large optical band gaps (2.8–3.1 eV) and highly stabilized ($-\Delta E_{LUMO}$ = 1.2–1.4 eV)/π-delocalized lowest unoccupied molecular orbitals (LUMOs) as compared to p-type DAcTTs. Symmetric functionalization was found to be important to enable strong intermolecular interactions in the solid-state. Single-crystal structural/packing analysis have revealed that all symmetrically functionalized low LUMO BTBT molecules show alternately stacked layers of "F–BTBT–F" and "S" with strong herringbone-like interactions (2.8–3.6 Å distances) between π-cores. The carbonyl functional groups adopt coplanar conformations with the BTBT π-backbone; however, the dicyanovinylenes are found to be twisted (47.5°). This conformational change at the molecular level is found to have unusual effects on the π-electron deficiencies (high-field ^{1}H NMR peaks and shielding effects, $-\Delta\delta_{Ar-H}$ = 0.4–0.5 ppm), thermal properties (lowered melting point, $-\Delta T_{mp}$ = 55 °C), frontier molecular orbital energetics (increased LUMOs, ΔE_{LUMO} = 0.2 eV), photophysical properties (PL quenching and free-rotor effect), and π-electronic structures (3D electron transporting BTBT···dicyanovinylene network and increased λ_e). Herein, dicyanovinylenes are demonstrated for the first time to yield electron transport in DAcTTs despite their twisted conformations. **D(C_7CC(CN)$_2$)-BTBT** becomes a rare example of an n-type DAcTT with an appreciable μ_e of 0.004 cm^2 V^{-1} s^{-1} (I_{on}/I_{off} = 10^6–10^7). Although a low energy delocalized LUMO, mainly governed by functional groups, is clearly required for electron transport, our results suggest that substituents are the key substructures to control intermolecular interactions in the charge transport direction and the relative electron *vs.* hole intramolecular reorganization energies. With the findings presented herein, we take the first step of establishing important and unique relationships between structure, various molecular properties, and semiconductivity in this new class of functionalized low LUMO BTBTs, and hope to stimulate further research on n-type DAcTTs in wide-ranging aspects of organic optoelectronics.

Conflicts of interest

There are no conflicts to declare.

Acknowledgements

H. U., R. O., and I. D. acknowledge support from the Scientific and Technological Research Council of Turkey (TUBITAK) grant number 216M430. M.-G. K. and K. A. acknowledge support from the National Research Foundation of Korea (NRF) grant number 2016K2A9A1A06924256. We thank Prof. E. Mutlugun and A. F. Yazici for their help with the photoluminescence measurements.

References

1 W. Wu, Y. Liu and D. Zhu, *Chem. Soc. Rev.*, 2010, **39**, 1489–1502.
2 J. E. Anthony, *Chem. Rev.*, 2006, **106**, 5028–5048.
3 K. Niimi, S. Shinamura, I. Osaka, E. Miyazaki and K. Takimiya, *J. Am. Chem. Soc.*, 2011, **133**, 8732–8739.
4 J. T. E. Quinn, J. Zhu, X. Li, J. Wang and Y. Li, *J. Mater. Chem. C*, 2017, **5**, 8654–8681.
5 B. Lim, H. Sun, J. Lee and Y.-Y. Noh, *Sci. Rep.*, 2017, **7**, 164.
6 R. Ozdemir, S. Park, İ. Deneme, Y. Park, Y. Zorlu, H. A. Alidagi, K. Harmandar, C. Kim and H. Usta, *Org. Chem. Front.*, 2018, **5**, 2912–2924.
7 E. K. Burnett, J. Ly, M. R. Niazi, L. Zhang, S. R. McCuskey, A. Amassian, D. Smilgies, S. C. B. Mannsfeld and A. L. Briseno, *Adv. Mater. Interfaces*, 2018, **5**, 1701607.
8 D. Khim, K.-J. Baeg, J. Kim, M. Kang, S.-H. Lee, Z. Chen, A. Facchetti, D.-Y. Kim and Y.-Y. Noh, *ACS Appl. Mater. Interfaces*, 2013, **5**, 10745–10752.
9 C. Ruiz, I. Arrechea-Marcos, A. Benito-Hernández, E. Gutierrez-Puebla, M. A. Monge, J. T. López Navarrete, M. C. Ruiz Delgado, R. P. Ortiz and B. Gómez-Lor, *J. Mater. Chem. C*, 2018, **6**, 50–56.

10 D. Zhao, J. Chen, B. Wang, G. Wang, Z. Chen, J. Yu, X. Guo, W. Huang, T. J. Marks and A. Facchetti, *J. Am. Chem. Soc.*, 2020, **142**, 5487–5492.
11 H. Huang, L. Yang, A. Facchetti and T. J. Marks, *Chem. Rev.*, 2017, **117**, 10291–10318.
12 A. Punzi, A. Operamolla, O. Hassan Omar, F. Brunetti, A. D. Scaccabarozzi, G. M. Farinola and N. Stingelin, *Chem. Mater.*, 2018, **30**, 2213–2217.
13 A. Facchetti, M. Mushrush, M. H. Yoon, G. R. Hutchison, M. A. Ratner and T. J. Marks, *J. Am. Chem. Soc.*, 2004, **126**, 13859–13874.
14 M. Mushrush, A. Facchetti, M. Lefenfeld, H. E. Katz and T. J. Marks, *J. Am. Chem. Soc.*, 2003, **125**, 9414–9423.
15 A. R. Murphy and J. M. J. Fréchet, *Chem. Rev.*, 2007, **107**, 1066–1096.
16 L. Zhang, N. S. Colella, B. P. Cherniawski, S. C. B. Mannsfeld and A. L. Briseno, *ACS Appl. Mater. Interfaces*, 2014, **6**, 5327–5343.
17 C. Liu, Y. Xu and Y.-Y. Noh, *Mater. Today*, 2015, **18**, 79–96.
18 Y.-Y. Noh, R. Azumi, M. Goto, B.-J. Jung, E. Lim, H.-K. Shim, Y. Yoshida, K. Yase and D.-Y. Kim, *Chem. Mater.*, 2005, **17**, 3861–3870.
19 Y. Liu, C. Di, C. Du, Y. Liu, K. Lu, W. Qiu and G. Yu, *Chem. – Eur. J.*, 2010, **16**, 2231–2239.
20 W. Jiang, Y. Li and Z. Wang, *Chem. Soc. Rev.*, 2013, **42**, 6113–6127.
21 X.-C. Li, H. Sirringhaus, F. Garnier, A. B. Holmes, S. C. Moratti, N. Feeder, W. Clegg, S. J. Teat and R. H. Friend, *J. Am. Chem. Soc.*, 1998, **120**, 2206–2207.
22 X. Gao, C. Di, Y. Hu, X. Yang, H. Fan, F. Zhang, Y. Liu, H. Li and D. Zhu, *J. Am. Chem. Soc.*, 2010, **132**, 3697–3699.
23 H. Usta and A. Facchetti, *Flexible Carbon-based Electronics*, Wiley-VCH Verlag GmbH & Co. KGaA, Weinheim, Germany, 2018, pp. 13–50.
24 M. L. Tang, A. D. Reichardt, P. Wei and Z. Bao, *J. Am. Chem. Soc.*, 2009, **131**, 5264–5273.
25 H. Klauk, *Chem. Soc. Rev.*, 2010, **39**, 2643–2666.
26 C. D. Sheraw, T. N. Jackson, D. L. Eaton and J. E. Anthony, *Adv. Mater.*, 2003, **15**, 2009–2011.
27 X. Zhan, A. Facchetti, S. Barlow, T. J. Marks, M. A. Ratner, M. R. Wasielewski and S. R. Marder, *Adv. Mater.*, 2011, **23**, 268–284.
28 T. Mori, T. Nishimura, T. Yamamoto, I. Doi, E. Miyazaki, I. Osaka and K. Takimiya, *J. Am. Chem. Soc.*, 2013, **135**, 13900–13913.
29 T. Mori, T. Oyama, H. Komiyama and T. Yasuda, *J. Mater. Chem. C*, 2017, **5**, 5872–5876.
30 J. Il Park, J. W. Chung, J. Y. Kim, J. Lee, J. Y. Jung, B. Koo, B. L. Lee, S. W. Lee, Y. W. Jin and S. Y. Lee, *J. Am. Chem. Soc.*, 2015, **137**, 12175–12178.
31 K. Takimiya, S. Shinamura, I. Osaka and E. Miyazaki, *Adv. Mater.*, 2011, **23**, 4347–4370.
32 Y. Yuan, G. Giri, A. L. Ayzner, A. P. Zoombelt, S. C. B. Mannsfeld, J. Chen, D. Nordlund, M. F. Toney, J. Huang and Z. Bao, *Nat. Commun.*, 2014, **5**, 3005.
33 K. He, S. Zhou, W. Li, H. Tian, Q. Tang, J. Zhang, D. Yan, Y. Geng and F. Wang, *J. Mater. Chem. C*, 2019, **7**, 3656–3664.
34 H. Usta, D. Kim, R. Ozdemir, Y. Zorlu, S. Kim, M. C. Ruiz Delgado, A. Harbuzaru, S. Kim, G. Demirel, J. Hong, Y.-G. Ha, K. Cho, A. Facchetti and M.-G. Kim, *Chem. Mater.*, 2019, **31**, 5254–5263.
35 A. Naibi Lakshminarayana, A. Ong and C. Chi, *J. Mater. Chem. C*, 2018, **6**, 3551–3563.
36 C. R. Newman, C. D. Frisbie, D. A. da Silva Filho, J.-L. Brédas, P. C. Ewbank and K. R. Mann, *Chem. Mater.*, 2004, **16**, 4436–4451.
37 J. Dhar, U. Salzner and S. Patil, *J. Mater. Chem. C*, 2017, **5**, 7404–7430.
38 C. Zhang, Y. Zang, F. Zhang, Y. Diao, C. R. McNeill, C. Di, X. Zhu and D. Zhu, *Adv. Mater.*, 2016, **28**, 8456–8462.
39 H. Usta, A. Facchetti and T. J. Marks, *Acc. Chem. Res.*, 2011, **44**, 501–510.
40 C.-Y. Yang, W.-L. Jin, J. Wang, Y.-F. Ding, S. Nong, K. Shi, Y. Lu, Y.-Z. Dai, F.-D. Zhuang, T. Lei, C.-A. Di, D. Zhu, J.-Y. Wang and J. Pei, *Adv. Mater.*, 2018, **30**, 1802850.
41 G. Wang, F. S. Melkonyan, A. Facchetti and T. J. Marks, *Angew. Chem., Int. Ed.*, 2019, **58**, 4129–4142.
42 D. Yang and D. Ma, *Adv. Opt. Mater.*, 2019, **7**, 1800522.
43 D. Ho, R. Ozdemir, H. Kim, T. Earmme, H. Usta and C. Kim, *ChemPlusChem*, 2019, **84**, 18–37.
44 H. Sun, L. Wang, Y. Wang and X. Guo, *Chem. – Eur. J.*, 2019, **25**, 87–105.
45 H. Sun, X. Guo and A. Facchetti, *Chem*, 2020, **6**, 1310–1326.
46 H. Ebata, T. Izawa, E. Miyazaki, K. Takimiya, M. Ikeda, H. Kuwabara and T. Yui, *J. Am. Chem. Soc.*, 2007, **129**, 15732–15733.
47 M. Grabolle, M. Spieles, V. Lesnyak, N. Gaponik, A. Eychmüller and U. Resch-Genger, *Anal. Chem.*, 2009, **81**, 6285–6294.
48 Y. Altintas, M. Y. Talpur, M. Ünlü and E. Mutlugün, *J. Phys. Chem. C*, 2016, **120**, 7885–7892.
49 M. M. J. Frisch, G. W. Trucks, H. B. Schlegel, G. E. Scuseria, H. A. Robb, J. R. Cheeseman, G. Scalmani, V. Barone, B. Mennucci, G. A. Petersson, J. L. Nakatsuji, M. Caricato, X. Li, H. P. Hratchian, A. F. Izmaylov, J. Bloino, G. Zheng, T. Sonnenberg, M. Hada, M. Ehara, K. Toyota, R. Fukuda, J. Hasegawa, M. Ishida, F. Nakajima, Y. Honda, O. Kitao, H. Nakai, T. Vreven, J. A. Montgomery, Jr., J. E. Peralta, R. Ogliaro, M. Bearpark, J. J. Heyd, E. Brothers, K. N. Kudin, V. N. Staroverov, J. Kobayashi, J. Normand, K. Raghavachari, A. Rendell, J. C. Burant, S. S. Iyengar, C. Tomasi, M. Cossi, N. Rega, J. M. Millam, M. Klene, J. E. Knox, J. B. Cross, V. Bakken, C. Adamo, J. Jaramillo, R. Gomperts, R. E. Stratmann, O. Yazyev, A. J. Austin, R. Cammi, P. Pomelli, J. W. Ochterski, R. L. Martin, K. Morokuma, V. G. Zakrzewski, G. A. Voth, J. V. Salvador, J. J. Dannenberg, S. Dapprich, A. D. Daniels, Ö. Farkas, J. B. Foresman, J. V. Ortiz, J. Cioslowski and D. J. Fox, *Gaussian 09, Revision C.01*, Gaussian Inc, Wallingford, CT, USA, 2010.
50 J.-L. Brédas, D. Beljonne, V. Coropceanu and J. Cornil, *Chem. Rev.*, 2004, **104**, 4971–5004.
51 B. Košata, V. Kozmik, J. Svoboda, V. Novotná, P. Vaněk and M. Glogarová, *Liq. Cryst.*, 2003, **30**, 603–610.

52 E. Jacques, M. Romain, A. Yassin, S. Bebiche, M. Harnois, T. Mohammed-Brahim, J. Rault-Berthelot and C. Poriel, *J. Mater. Chem. C*, 2014, **2**, 3292–3302.
53 H. Usta, C. Risko, Z. Wang, H. Huang, M. K. Deliomeroglu, A. Zhukhovitskiy, A. Facchetti and T. J. Marks, *J. Am. Chem. Soc.*, 2009, **131**, 5586–5608.
54 M. Romain, M. Chevrier, S. Bebiche, T. Mohammed-Brahim, J. Rault-Berthelot, E. Jacques and C. Poriel, *J. Mater. Chem. C*, 2015, **3**, 5742–5753.
55 S. Inoue, H. Minemawari, J. Tsutsumi, M. Chikamatsu, T. Yamada, S. Horiuchi, M. Tanaka, R. Kumai, M. Yoneya and T. Hasegawa, *Chem. Mater.*, 2015, **27**, 3809–3812.
56 V. S. Vyas, R. Gutzler, J. Nuss, K. Kern and B. V. Lotsch, *CrystEngComm*, 2014, **16**, 7389–7392.
57 J. L. Brédas, G. B. Street, B. Thémans and J. M. André, *J. Chem. Phys.*, 1985, **83**, 1323–1329.
58 A. Bondi, *J. Phys. Chem.*, 1964, **68**, 441–451.
59 R. Ozdemir, D. Choi, M. Ozdemir, G. Kwon, H. Kim, U. Sen, C. Kim and H. Usta, *J. Mater. Chem. C*, 2017, **5**, 2368–2379.
60 R. D. McCullough, *Adv. Mater.*, 1998, **10**, 93–116.
61 D. R. Lide, *CRC Handbook of Chemistry and Physics*, CRC Press, Boca Raton, FL, 85th edn, 2004.
62 S. C. Lee, J. Heo, H. C. Woo, J. A. Lee, Y. H. Seo, C. L. Lee, S. Kim and O. P. Kwon, *Chem. – Eur. J.*, 2018, **24**, 13706–13718.
63 B. Chen, Y. Ding, X. Li, W. Zhu, J. P. Hill, K. Ariga and Y. Xie, *Chem. Commun.*, 2013, **49**, 10136–10138.
64 J. Shao, S. Ji, X. Li, J. Zhao, F. Zhou and H. Guo, *Eur. J. Org. Chem.*, 2011, 6100–6109.
65 X. Sun, T. D. James and E. V. Anslyn, *J. Am. Chem. Soc.*, 2018, **140**, 2348–2354.
66 M. G. Kim, M. G. Kanatzidis, A. Facchetti and T. J. Marks, *Nat. Mater.*, 2011, **10**, 382–388.
67 G. Kwon, K. Kim, B. D. Choi, J. Roh, C. Lee, Y.-Y. Noh, S. Seo, M.-G. Kim and C. Kim, *Adv. Mater.*, 2017, **29**, 1607055.
68 H. Lee, D. Lee, D. H. Sin, S. W. Kim, M. S. Jeong and K. Cho, *NPG Asia Mater.*, 2018, **10**, 469–481.
69 J.-W. Lee, M. J. Sung, D. Kim, S. Lee, H. You, F. S. Kim, Y.-H. Kim, B. J. Kim and S.-K. Kwon, *Chem. Mater.*, 2020, **32**, 2572–2582.
70 Y. Li, M. Kim, Z. Wu, C. Lee, Y. W. Lee, J.-W. Lee, Y. J. Lee, E. Wang, B. J. Kim and H. Y. Woo, *J. Mater. Chem. C*, 2019, **7**, 1681–1689.
71 K.-J. Baeg, M. Binda, D. Natali, M. Caironi and Y.-Y. Noh, *Adv. Mater.*, 2013, **25**, 4267–4295.
72 Y. Liu, J. Zhao, Z. Li, C. Mu, W. Ma, H. Hu, K. Jiang, H. Lin, H. Ade and H. Yan, *Nat. Commun.*, 2014, **5**, 5293.
73 Y. Zhao, Y. Guo and Y. Liu, *Adv. Mater.*, 2013, **25**, 5372–5391.
74 Y. Sui, Y. Deng, T. Du, Y. Shi and Y. Geng, *Mater. Chem. Front.*, 2019, **3**, 1932–1951.
75 J. Cornil, D. Beljonne, J.-P. Calbert and J.-L. Brédas, *Adv. Mater.*, 2001, **13**, 1053–1067.
76 J. A. Letizia, A. Facchetti, C. L. Stern, M. A. Ratner and T. J. Marks, *J. Am. Chem. Soc.*, 2005, **127**, 13476–13477.
77 G. R. Hutchison, M. A. Ratner and T. J. Marks, *J. Am. Chem. Soc.*, 2005, **127**, 2339–2350.
78 O. Kwon, V. Coropceanu, N. E. Gruhn, J. C. Durivage, J. G. Laquindanum, H. E. Katz, J. Cornil and J. L. Brédas, *J. Chem. Phys.*, 2004, **120**, 8186–8194.
79 N. Metri, X. Sallenave, C. Plesse, L. Beouch, P.-H. Aubert, F. Goubard, C. Chevrot and G. Sini, *J. Phys. Chem. C*, 2012, **116**, 3765–3772.